Volume 11
Number 9
7 May 2021
Pages 2969–3296

Catalysis Science & Technology

rsc.li/catalysis

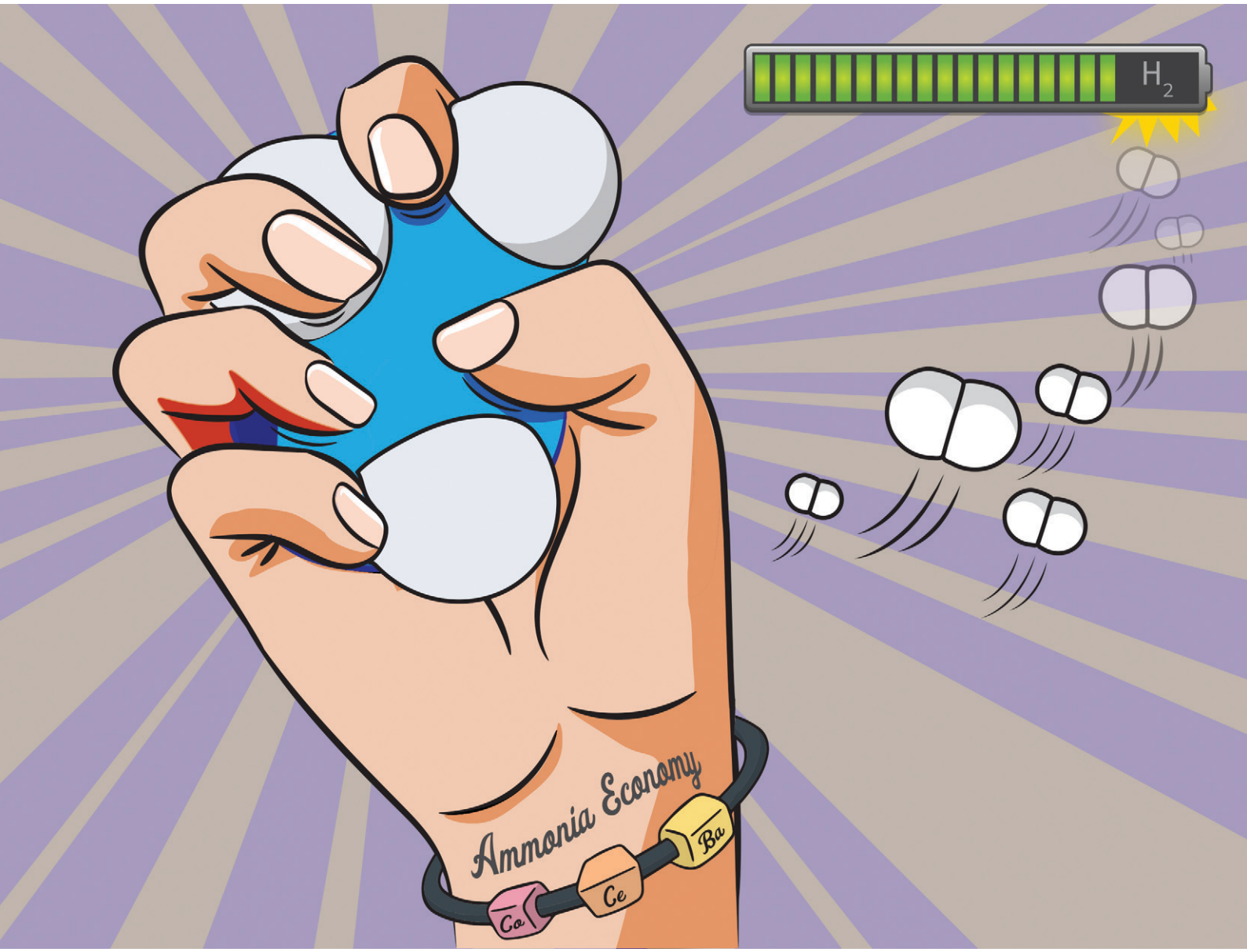

ISSN 2044-4761

ROYAL SOCIETY OF CHEMISTRY

PAPER
Jorge Gascon *et al.*
Development of a Ba–CoCe catalyst for the efficient and stable decomposition of ammonia

Catalysis Science & Technology

ROYAL SOCIETY OF CHEMISTRY

PAPER

View Article Online
View Journal | View Issue

Cite this: *Catal. Sci. Technol.*, 2021, **11**, 3014

Development of a Ba–CoCe catalyst for the efficient and stable decomposition of ammonia†

Natalia Morlanés,‡[a] Salvador Sayas,‡[a] Genrikh Shterk,[a] Sai P. Katikaneni,[b] Aadesh Harale,[b] Bandar Solami[b] and Jorge Gascon *[a]

Received 3rd December 2020,
Accepted 5th March 2021

DOI: 10.1039/d0cy02336a

rsc.li/catalysis

Barium-promoted cobalt–cerium catalysts prepared by coprecipitation are efficient and stable at decomposing ammonia. Catalysts with the optimal composition show very similar activity and better stability than benchmark solids containing Ru. Characterization studies reveal that cerium plays a key role as a structural promoter, increasing cobalt dispersion and preventing sintering. These features translate into a very active and stable catalyst. Kinetic analysis shows a decrease in the apparent activation energy upon Ba promotion and a decrease in the negative hydrogen reaction order, highlighting the role of the alkaline earth metal in alleviating the negative effect of hydrogen and reducing the hydrogenation properties of cobalt, which results in further improvement of the catalytic activity.

Introduction

The search for cleaner energy carriers points to hydrogen as the most interesting candidate.[1–3] However, for the "hydrogen economy" to become a reality, the safe and economical storage of this gas is of the utmost importance.[1] In this context, the use of ammonia as an efficient hydrogen carrier will most likely play an important role. The main advantages of ammonia are (i) a well-established production and distribution technology, (ii) high volumetric and gravimetric energy density and (iii) the fact that ammonia can be catalytically decomposed into CO_x-free hydrogen.[2–4]

However, the best catalytic systems reported for ammonia decomposition are based on ruthenium, which strongly limits the large-scale implementation of this technology.[5–8] This issue has generated interest in developing alternative catalysts based on sustainable and available non-noble metals, mainly iron, cobalt or nickel.[5,8] These transition metals, however, show good catalytic activity only at high temperatures (>600 °C) and are not able to meet the U.S. DOE specifications for hydrogen storage (99% conversion at 450 °C).[9] Therefore, more research is needed into transition-metal-based catalysts to meet this target.

Cobalt offers advantages compared to iron or nickel, and it is expected to be the most active transition metal for ammonia decomposition, especially at low reaction temperatures.[4,10,11] This is associated to the weaker nitrogen binding energy of cobalt compared to iron or nickel, especially under high ammonia concentration, resulting in lower activation energy.[7] Metallic cobalt has been widely proposed as the active phase for ammonia decomposition.[7,8] In general, Co-based catalysts are strongly affected by the physical and chemical properties of the support (*e.g.* basicity and electron conductivity) as well as by the presence of promoters.[12–18] Likewise, the preparation method and pretreatment conditions are critical parameters altering activity and stability.[19] The use of high surface area supports, especially with basic properties, by the addition of alkali or alkaline earth promoters, resulted in higher metal dispersion; the most active cobalt particle size has been reported within the range of 10–20 nm.[12,13,20,21] In addition, the use of carbon supports with an appropriate metal–support interaction with cobalt resulted in improved electron transfer and consequently a reduction in the nitrogen desorption energy, increasing the activity.[22–27] In spite of these insights, only moderate activity has been found at temperatures >600 °C.

Here, we report the synthesis, characterization and catalytic performance of cobalt–cerium (CoCe)-based solids. When promoted with small amounts of Ba, 0.5% Ba–CoCe(80/20), the outstanding catalytic performance at 450 °C is comparable to that of a Ru-based reference catalyst. Characterization studies reveal that cerium plays a key role as a structural promoter, increasing cobalt dispersion and preventing sintering.

[a] *KAUST Catalysis Center (KCC), King Abdullah University of Science and Technology (KAUST), Thuwal 23955-6900, Saudi Arabia.*
E-mail: Jorge.Gascon@kaust.edu.sa
[b] *Carbon Management R&D Division, Research and Development Center, Saudi Aramco, Dhahran, 31311 Saudi Arabia*

† Electronic supplementary information (ESI) available: Experimental details of synthesis, characterization, and catalytic studies. See DOI: 10.1039/d0cy02336a

‡ These authors contributed equally to this work.

Experimental

Cobalt-based catalysts, Ba–CoCe, were synthesized by coprecipitation. In the first step, cobalt and cerium precursors were coprecipitated in basic medium in the presence of carbonate, using a Co/Ce molar ratio in the range 50/50 to 95/5. After calcination of the samples at 500 °C for 3 h, barium was incorporated by wet impregnation to achieve barium loadings in the range 0.25–1 wt%. Details related to the materials and methods used for the synthesis of the catalysts in the present study are provided in the ESI.† The CoCe samples were named CoCe(X/Y), and the CoCe samples with Ba incorporated as Z% Ba–CoCe(X/Y), where (X/Y) represents the Co/Ce molar ratio and Z is the loading (wt%) of barium.

Ru-based catalysts were used as reference in the present study,[28] supported on CaO, MgO and CeO_2, with 3 wt% Ru loading, promoted with K (10 wt%), and prepared according to previously reported procedures detailed in the ESI.†[29–31] The Ru catalysts were named 3%Ru–10%K/CaO, 3%Ru–10%K/MgO, and 3%Ru–10%K/CeO_2.

For comparison purposes, several samples were prepared by impregnation of different cobalt loadings (2–30 wt%) on commercially available CeO_2 support. Similarly, the samples followed the same calcination procedure as the samples prepared by coprecipitation, 3 h at 550 °C. These samples were named x% Co/CeO_2, where x is the loading (wt%) of cobalt.

The composition of the samples was analyzed by ICP measurements on a Thermo-Electron 3580 instrument. Nitrogen physisorption was carried out on an ASAP 2020 instrument (Micromeritics Co.). X-ray powder diffraction (XRD) measurements were carried out using a Bruker D8 instrument in Bragg–Brentano configuration using Cu Kα radiation. Transmission electron microscopy (HR-TEM) images were collected using a Titan Themis-Z microscope from Thermo-Fisher Scientific operated at an accelerating voltage of 300 kV and beam current of 0.5 mA. Hydrogen temperature-programmed reduction (H_2-TPR) studies were performed in an Altamira instruments setup. The surface area of metallic Co was evaluated by H_2 chemisorption (H_2-TPD) using a fully automated flow AutoChem 2920 system (Micromeritics Instrument Co.) coupled with a mass spectrometer. The surface chemical compositions and chemical states were analyzed by *in situ* NAP-XPS measurements carried out with an EnviroESCA spectrometer (SPECS GmbH) equipped with a monochromatic Al Kα X-ray source ($h\nu$ = 1486.6 eV) operating at 42 W and X-ray emission at 3.00 mA.

Ammonia decomposition catalytic tests were carried out in a PID Microactivity Reference system using a continuous fixed-bed stainless steel reactor coated with alumina to avoid any activity of the reactor construction material. Prior to the activity measurement, the catalysts (200 mg pelletized between 300 μm and 500 μm and diluted with 1 g of SiC) were reduced/activated *in situ* with hydrogen (25 mL min^{-1}) at 500 °C for 3 h. The catalytic performance was evaluated at different temperatures in the range 250–550 °C. Details of the experimental setup used for this process and the experiments conducted are provided in the ESI† (Fig. S1).

Results and discussion

Catalyst structural characterization

The composition of the catalyst precursors obtained by precipitation and subsequent calcination was analyzed by ICP. The Co, Ce and Ba contents are shown in Table 1 along with their calculated specific surface area (S_{BET}) and pore volume (V_p). The quantified composition matches the nominal composition, corroborating the successful coprecipitation of Co and Ce and the incorporation of Ba *via* impregnation. The specific surface area and pore volume increased significantly as a result of the addition of cerium in relation to the pure cobalt oxide (Co without Ce) sample. This increase in surface area upon incorporation of Ce suggests that cerium plays a role of structural promoter, which improves the surface of the catalyst precursors and prevents the sintering of these materials during calcination (*vide infra*).[32]

The phase composition of the materials in their oxidized (after calcination) and reduced form (after activation/reduction and after the catalytic tests) was determined using X-ray powder diffraction. The diffraction patterns for the samples after calcination at 550 °C are shown in Fig. 1. In all the samples with different CoCe molar ratios, cobalt in the form of Co_3O_4 (JCPDS 42-1467) and Ce as CeO_2 (JCPDS 34-0394) are observed. In addition, in the sample promoted with barium (Ba–CoCe), crystalline Ba phases are not observed, probably due to the very small Ba loading (0.5% wt). In the diffraction pattern of samples after reduction in hydrogen at 500 °C (Fig. 2) and after the catalytic tests (Fig. S2 and S3†), metallic cobalt is the only cobalt phase observed (JCPDS 15-0806 for the fcc phase and 05-0727 for the hcp phase),[32,33] while Ce is present as CeO_2. As expected, during catalyst activation prior to the catalytic tests, Co_3O_4 is reduced to metallic cobalt. It has been previously observed that the addition of Ce stabilizes the hcp phase up to the temperature of 600 °C,[32–34] even though the allotropic transformation from hcp to fcc phase occurs at 420 °C.[33,35] No significant change in the XRD pattern is observed after the activity

Table 1 Composition and S_{BET} of Ba–CoCe catalysts prepared by coprecipitation

	Co (wt%)	Ce (wt%)	Ba (wt%)	BET ($m^2\ g^{-1}$)	V_p ($cm^3\ g^{-1}$)
Co (without Ce)	72.1	—		37	0.15
CoCe(95/5)	65.3	8.0		46	0.18
CoCe(90/10)	53.0	14.2		50	0.20
CoCe(80/20)	41.7	23.7		55	0.22
CoCe(70/30)	30.2	30.1		59	0.24
CoCe(50/50)	17.9	42.1		63	0.25
0.5Ba/CoCe(80/20)	41.4	23.5	0.45	58	0.23

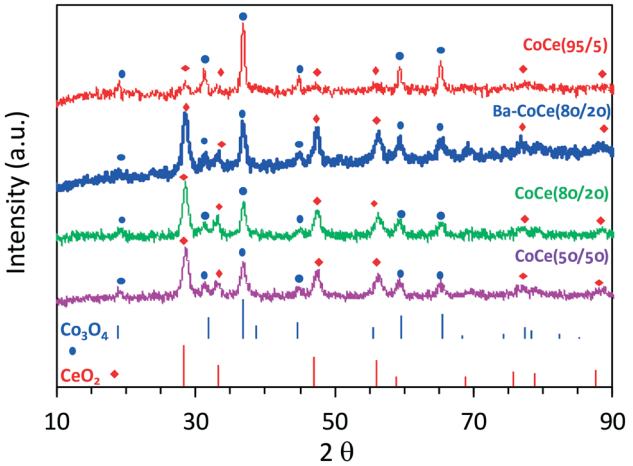

Fig. 1 XRD patterns of CoCe catalysts with different CoCe molar ratios after calcination in air at 550 °C for 3 h.

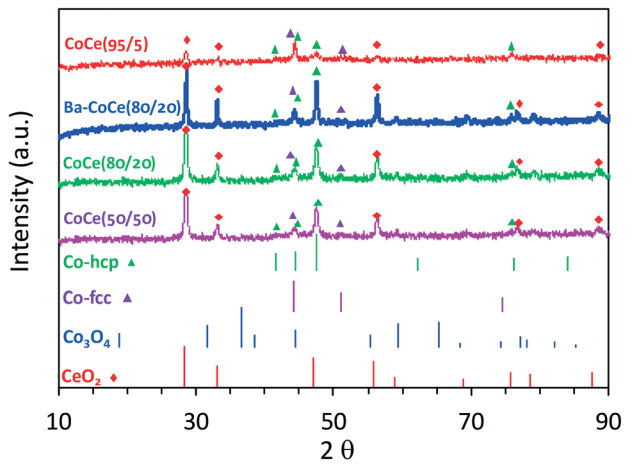

Fig. 2 XRD patterns of CoCe catalysts with different CoCe molar ratios, after activation treatment under hydrogen at 500 °C for 3 h.

measurements (Fig. S2 and S3†) compared to the structure of the samples after the activation treatment (Fig. 2), already anticipating the stability of the structure and of the catalytic properties of the materials.

The reducibility of cobalt oxide to metallic Co, occurring during the activation treatment under hydrogen atmosphere at 500 °C, was investigated by temperature-programmed reduction (H_2-TPR) in order to understand the influence of cerium and barium. TPR curves for cobalt oxide (without Ce) for a system containing a mixture of cobalt and cerium (Co/Ce) and for the sample promoted with barium (Ba–CoCe) are presented in Fig. 3. For the cobalt oxide sample (without Ce), there are two signals; the first one, in the range of 175–300 °C, is associated to the reduction of Co_3O_4 to CoO; the second one, at 330–480 °C, corresponds to a further reduction from CoO to Co, in agreement with the literature.[36] The presence of Ce or Ba results in a broadening of the two signals, associated with the interaction of the components in the system.[32,37,38] In general, Ce addition slightly shifts the

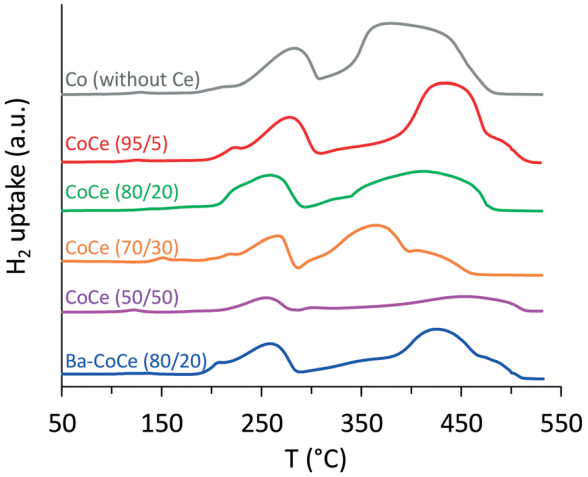

Fig. 3 H_2-TPR curves for CoCe catalysts with different CoCe molar ratios and promoted with Ba.

first reduction event to a lower temperature, while the second reduction event starts and is extended to higher temperatures.[32,38,39]

From the hydrogen uptakes evaluated by the H_2-TPR measurements (Table 2), it is concluded that Co_3O_4 is not completely reduced to cobalt metal for these samples under the TPR conditions, with smaller reduction degrees achieved for the samples with higher cerium content. This result suggests that Ce retards the reduction of cobalt oxide, in agreement with previous studies.[32,38,39] On the other hand, the addition of Ba results in an increase of the H_2 uptake, and a higher reduction degree is observed. Therefore, we can conclude that barium facilitates the reduction of cobalt and/or cerium. The reduction of CeO_2 in the presence of Co as a result of the hydrogen spillover from metallic cobalt to ceria has been previously reported.[32,39,40] In this case, part of the H_2 uptake would correspond to the reduction of ceria, resulting in a slightly lower reduction degree for Co with respect to the values shown in Table 2.

In order to accurately evaluate the surface of the active phase (metallic Co), H_2 chemisorption experiments were conducted.[32,37,38] Based on the amount of chemisorbed hydrogen and assuming a spherical model for the Co crystallites, the surface area of the active phase (S_{Co}) was estimated. The S_{Co} values, evaluated after the reduction of

Table 2 H_2 uptake during H_2-TPR and reduction degree of Ba–CoCe catalysts prepared by coprecipitation

	H_2 consumption (mmol g^{-1})	Cobalt reduction degree (%)	1st peak (%)	2nd peak (%)
Co (without Ce)	15.4	82.6	27.9	72.1
CoCe(95/5)	13.9	82.5	27.9	72.1
CoCe(80/20)	9.0	83.8	31.4	68.6
CoCe(70/30)	5.7	73.1	31.2	68.8
CoCe(50/50)	3.7	79.4	32.3	67.7
0.5Ba/CoCe(80/20)	9.2	85.9	28.2	71.8

Table 3 H_2 chemisorption measurements and S_{Co} for catalysts of different CoCe molar ratios and promoted with Ba

Catalyst	H_2 chemisorption ($\mu mol\ g^{-1}$)	Co (%) dispersion	S_{Co} ($m^2\ g^{-1}$)
Co (without Ce)	1.2	0.01	0.04
CoCe (95/5)	87.9	0.79	2.87
CoCe (80/20)	120.7	1.71	3.95
CoCe(70/30)	41.0	0.80	1.34
CoCe(50/50)	12.6	0.42	0.41
0.5Ba/CoCe(80/20)	136.3	1.94	4.45

the different catalysts at 550 °C, are presented in Table 3, and the H_2-desorption curves are shown in Fig. S4.† S_{Co} strongly depends on the composition, with a clear maximum for sample CoCe(80/20). When this catalyst is further promoted with Ba (Ba–CoCe), the largest surface of the active phase was obtained. The sequence of S_{Co} values for reduced catalysts is as follows: S_{Co} (Ba–CoCe) > S_{Co} (CoCe) > S_{Co} (Co, without Ce). A CeO_2 sample prepared by the same precipitation and calcination protocols was analyzed after activation/reduction under H_2 at 550 °C to corroborate that H_2 was not chemisorbed under the experimental conditions.

The surface chemical compositions and chemical states were revealed by *in situ* XPS. Fig. 4 shows the XPS spectra of Ce 3d, O 1s and Co 2p of CoCe(80/20) catalysts after calcination at 550 °C and after reduction treatment at 500 °C for 2 h. XPS spectra of the Ce 3d region are composed of five doublets: v_0 (881.6 eV), u_0 (899.1 eV), v (882.9 eV), u (901.2 eV), v' (885.3 eV), u' (903.0 eV), v'' (888.9 eV), u'' (907.7 eV), v''' (898.1 eV) and u''' (916.7 eV).[40–42] v_0, v', u_0 and u' are assigned to Ce^{3+}; the rest of the doublets are assigned to Ce^{4+}. The Ce^{3+}/Ce^{4+} ratio slightly increases after the reduction treatment (Table 4), consistent with a partial reduction of the CeO_2, in agreement with previously reported observations.[32,39] Slightly more CeO_2 has been reduced in the case of the sample without Ba. In the Ce 3d spectrum corresponding to the sample with Ba, a slight broadening of the peaks is observed that could be related to a decrease in the ceria particle size. In order to analyze the surface oxygen species, the O 1s spectra can be deconvoluted into three peaks centered at 529.5, 530.9 and 532.7 eV (Fig. 4). The peaks at 529.5 and 530.9 eV are attributed to the lattice oxygen in Co oxides (CoO, Co_3O_4) and CeO_2, respectively, while the peak at 532.7 eV is attributed to surface adsorbed oxygen species. Finally, the Co 2p energy spectrum shows the bond energy peaks at 779.4 eV and 780.5 eV, which can be ascribed to Co_3O_4.[41,43] After the calcination treatment, Co_3O_4 is the main component, with Co^{2+} and Co^{3+} oxidation states, in agreement with the phase observed by XRD (Fig. 1). After the reduction, we can observe a peak at 778.1 eV, assigned to metallic Co, together with CoO peaks, suggesting that Co species might be present in Co^0 and Co^{2+} oxidation states in the CoCe(80/20) catalysts after the hydrogen treatment. Furthermore, there is no significant shift in the peak assigned to Co^0 in the samples CoCe(80/20) and 0.5Ba/CoCe(80/20), indicating that the addition of Ba to the CoCe

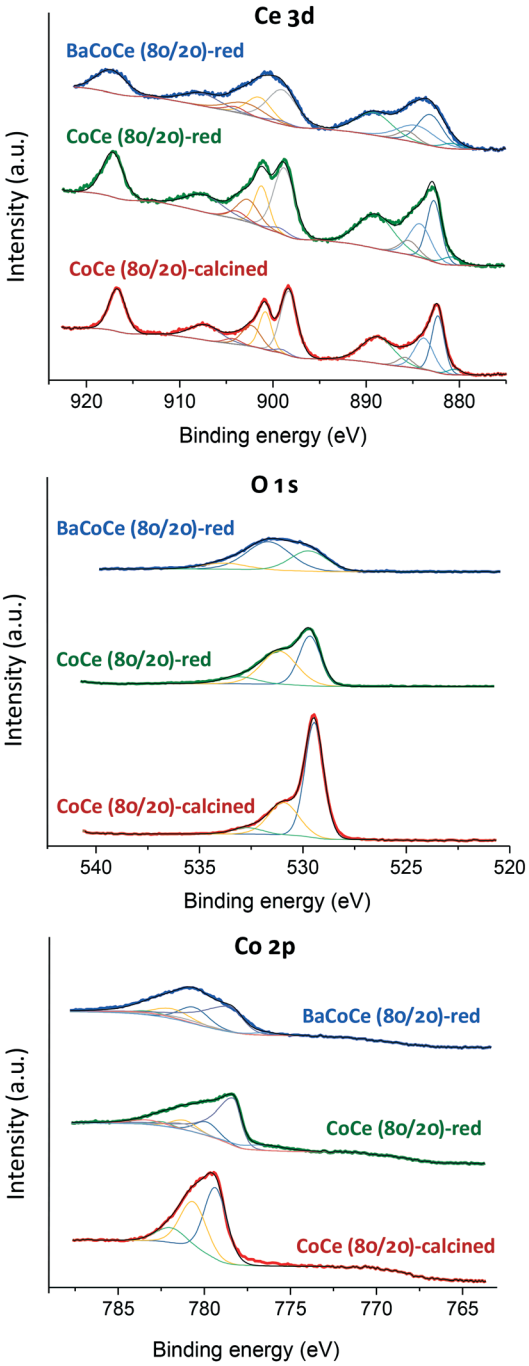

Fig. 4 XPS curve-fitting of the Ce 3d, O 1s and Co 2p spectra for CoCe(80/20)-calcined and reduced and 0.5Ba/CoCe(80/20) reduced catalysts.

Table 4 Summary of the XPS data for CoCe(80/20) calcined and reduced and 0.5Ba/CoCe(80/20) reduced catalysts

Catalyst	Co (at%)	Ce (at%)	O (at%)	Ba (at%)	Co^0/Co_{total}	Ce^{3+}/Ce^{4+}
CoCe(80/20)-calc.	12.0	5.8	72.5			0.063
CoCe(80/20)-red	11.8	10.1	66.3		0.76	0.096
0.5Ba/CoCe(80/20)-r	10.7	7.1	55.1	0.9	0.62	0.085

catalyst did not affect the binding energy. The Co^0/Co_{total} ratio is slightly smaller in the sample with Ba, suggesting that less Co is in the metallic state in this sample. This is in contrast with the smaller oxygen peak corresponding to the cobalt oxide lattice oxygen (529.5 eV) for the same sample, which would point to a higher reduction degree of the cobalt oxide in this sample. Furthermore, for both samples the Co^0/Co_{total} ratio is slightly smaller than the reduction degrees observed by H_2-TPR (Table 2), corroborating that part of the H_2 uptake observed for the H_2-TPR corresponds to the reduction of the CeO_2.

The local structures of the Co/Ce and Ba–Co/Ce catalysts were evaluated using high-angle annular darkfield scanning transmission electron microscopy (HAADF-STEM) and energy-dispersive X-ray (EDX) spectroscopy. Representative TEM images for Co/Ce(80/20) and Ba–Co/Ce(80/20) catalysts, after the activation treatment under hydrogen at 500 °C for 3 h, are shown in Fig. 5 and 6. Additional TEM images for sample Co/Ce(90/10) can be found in Fig. S5.† Nearly spherical shaped cobalt nanoparticles with a broad particle size distribution in the range of 5 to 30 nm are observed. In general, the elemental mapping shows that Ce is in the form of aggregates located around the Co nanoparticles. This structure suggests that the addition of Ce inhibited the growth of Co particles and therefore Ce is able to improve the Co dispersion by preventing Co aggregation. These features are strongly related with the increase in the activity and the stability of the catalytic performance experimentally observed (*vide infra*). In the 0.5Ba–Co/Ce(80/20) catalysts (Fig. 6), while mapping shows that the Ba dispersion is not homogeneous, the addition of Ba has a particular effect on the ceria dispersion, resulting in the formation of extremely small-sized Ce clusters decorating the surface of the cobalt nanoparticles.

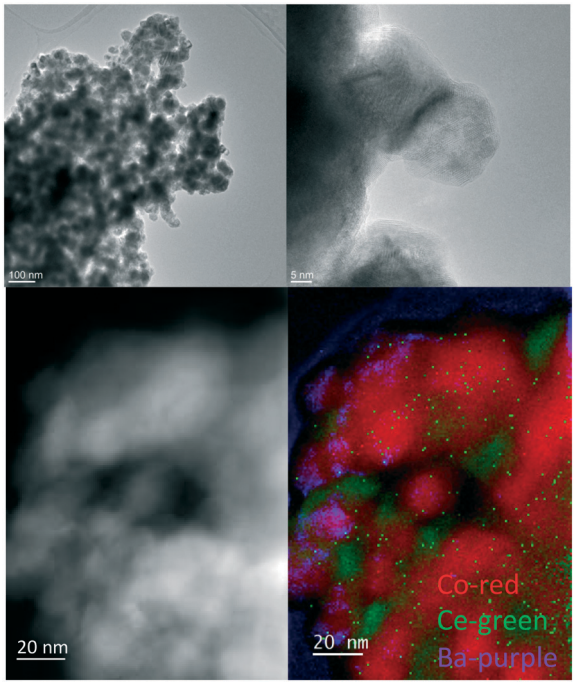

Fig. 6 HAADF-STEM and EDX for 0.5%Ba–CoCe(80/20) after activation under hydrogen at 500 °C. Co (red), Ce (green), Ba (purple).

In summary, characterization suggests that cerium acts as a structural promoter, improving the specific surface area (S_{BET}) and preventing cobalt sintering during reduction and

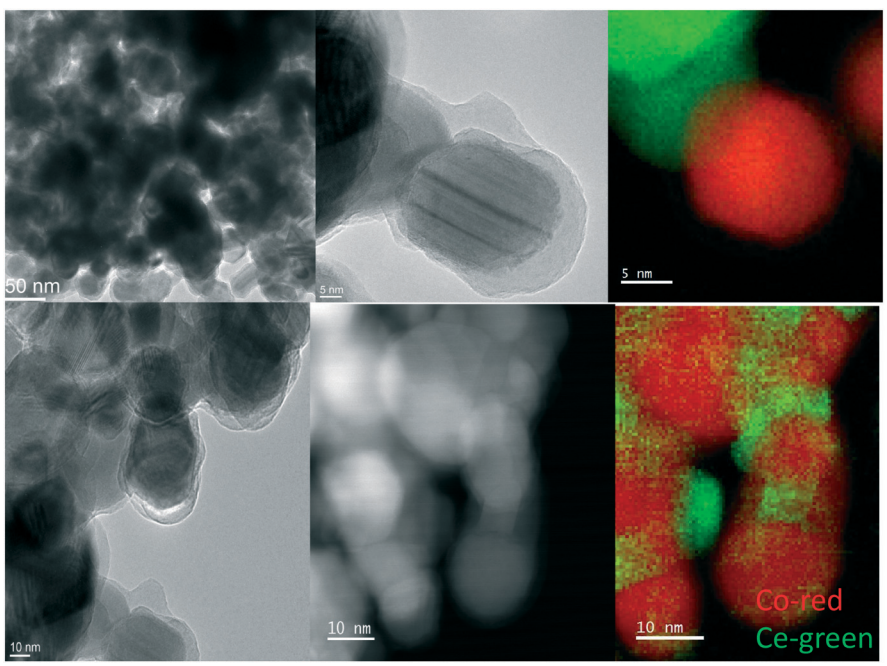

Fig. 5 Representative images for CoCe(80/20) after activation under hydrogen 500 °C 3 h, high-angle annular dark-field scanning transmission electron microscopy (HAADF-STEM) and energy-dispersive X-ray (EDX) spectroscopy. Elemental mapping: Co (red), Ce (green).

reaction conditions. The addition of barium results in an enhancement in the dispersion of cerium and helps in the development of more active surface area of metallic cobalt.

Catalytic performance

In order to successfully develop an efficient catalyst for the reaction of interest, the activity and stability of the different catalysts were evaluated in a fixed-bed plug flow reactor (ESI†). A number of reference catalysts were added to the testing for the sake of benchmarking and better understanding the systems at hand: (i) a state-of-the-art Ru-based solid and (ii) several additional catalysts prepared by Co impregnation on commercially available CeO_2. Fig. 7 shows ammonia conversion profiles as a function of reaction temperature. Fig. 7A includes the effect of Co loading in samples prepared by impregnation on CeO_2. Fig. 7B shows the effect of the method of incorporation of cobalt on the samples with different Co loadings (20–30% wt), prepared by impregnation and coprecipitation. Fig. 7C shows the effect of the Co/Ce molar ratio on the samples prepared by coprecipitation. Finally, the effect of Ba addition to the CoCe(80/20) sample prepared by coprecipitation is shown in Fig. 7D. Overall, the results demonstrate how the preparation method and promotion allow bringing the performance of Co catalysts close to that of the Ru-based benchmark, with the conversion gap at 450 °C being drastically reduced from a 74% difference to a mere 11%.

Fig. 7A shows an increase in ammonia conversion with higher Co loading up to 20% on samples prepared *via* impregnation, while further increase in the Co loading results in a dramatic decrease in activity. A different trend is found for samples prepared *via* coprecipitation; as shown in Fig. 7B, the samples with a 30 wt% Co loading show higher activity than those with a 20 wt% loading. This observation suggested that coprecipitation method would allow the incorporation of higher amounts of Co in the catalyst. Further optimization in Fig. 7C demonstrates that catalysts with a Co/Ce molar ratio of 80/20 (~42 wt% Co) show the optimal performance in terms of activity. Although Co/Ce(90/10) or (95/5) showed

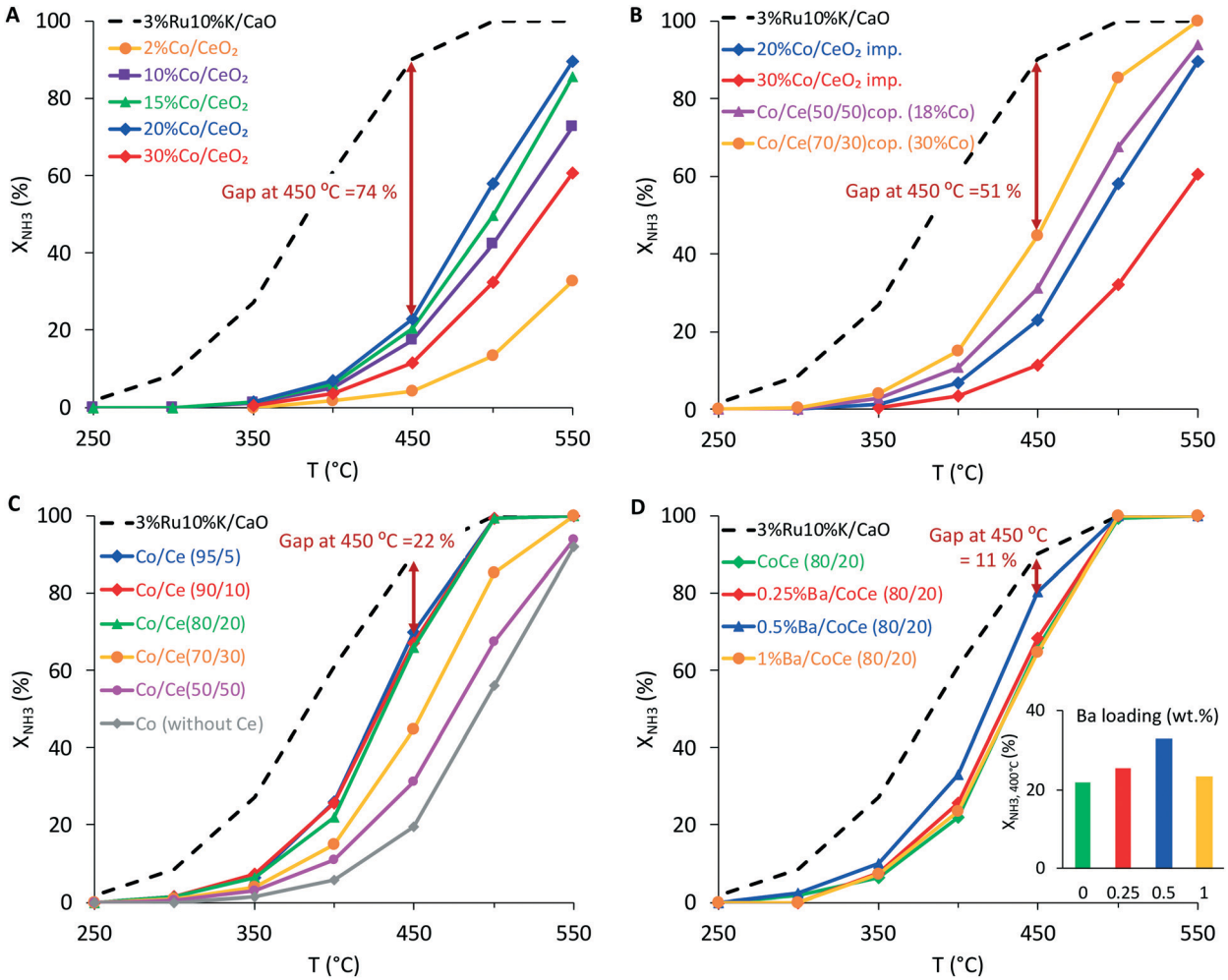

Fig. 7 Catalytic performance of CoCe catalysts in ammonia decomposition reaction. Conversion profiles *versus* reaction temperature. (A) Effect of Co loading (samples *via* impregnation); (B) coprecipitation *versus* impregnation method; (C) effect of Co/Ce molar ratio; (D) Ba promoter loading influence. Reaction conditions: P = 1 atm; T = 250–550 °C; NH_3 flow rate 30 Nml min^{-1}; W_{cat} = 200 mg; WHSV = 9000 mL g^{-1} h^{-1}.

similar activity, the catalyst with the molar ratio of 80/20 was selected as the most cost-effective catalyst taking into account the prices of Co and Ce. Additional promotion with different amounts of Ba in Fig. 7D shows an optimal promoter loading of 0.5 wt%. It is worth mentioning that for the optimized composition, only a gap of 11% in conversion when compared to the state-of-the-art Ru catalyst was observed. The catalytic performance of other Ru-based catalysts is shown in Fig. S6† for comparison purposes. The catalytic performance was also analysed by means of the reaction rates expressed per gram of Co (Fig. S7 and S8†), for the catalysts shown in Fig. 7A and B, in order to better understand the effect of the preparation method. Fig. S7† clearly shows the benefit of the coprecipitation method to incorporate higher loadings of cobalt.

A control experiment with only CeO_2 resulted in no catalytic activity, confirming that ammonia decomposition takes place only at Co sites.

We tried to further optimize the catalyst composition by performing the coprecipitation step in the presence of other elements suggested in the literature to improve Co catalytic activity, such as Al or Ca,[12,15,19] but this resulted in less active catalysts (Fig. S9†). For instance, ceria was similarly found to better improve the catalytic activity of Ru compared to alumina or magnesia.[44] Additionally, other alkali metals such as K and Cs[21,45] were incorporated by impregnation, but no improvement of the activity was observed (Fig. S10†), in agreement with previous studies,[46] corroborating that Ba is a better promoter for Co than K or Cs.[32,37,47,48]

From the observed catalytic activity and in-depth characterization, we conclude that there is a strong correlation between accessible Co surface area and catalytic performance (see Table 3 and Fig. 7), with only CoCe(95/5) falling out of that trend. This discrepancy might be related with the difference in the ratio between the two metallic cobalt phases observed in the XRD patterns of this sample (Fig. 2), fcc (signal 44.4°) and hcp (signal 47.6°): it should not be disregarded that reactivity might be different for these two phases, as has been shown for other Co-catalyzed reactions such as Fischer Tropsch synthesis.[49]

The coprecipitation of cobalt with different ratios of cerium allows the preparation of catalysts with very high content of cobalt while maximizing dispersion and preventing agglomeration, even under reaction conditions. Indeed, long-term stability tests on the best-performing catalyst (0.5%Ba–CoCe(80/20), Fig. 8) demonstrate no deactivation for at least 100 hours under reaction conditions and better stability than the Ru-based sample. These results are in line with the high thermal stability observed for similar CoCe-based solids.[32,37,38,50] To the best of our knowledge, 0.5%Ba–Co/Ce(80/20) is not only among the most active cobalt-based catalysts reported in the literature[12–26] (see Table S1† for a comparison) but its performance is also comparable to that of the Ru-based catalysts.

Last but not least, kinetic studies at atmospheric pressure were performed for CoCe(80/20) and 0.5%Ba–CoCe(80/20) in order to elucidate the effect of barium from a kinetic point of view (Fig. 9). Arrhenius plots for the different catalysts under study (Fig. S11†) showed no effect of the Co/Ce molar ratio on the apparent activation energy, always in the order of 90 kJ mol^{-1}, calculated from the slope of the plots. Introduction of Ba (Fig. 9A) results in a decrease in the apparent activation energy of *circa* 10 kJ mol^{-1} along with a decrease in the negative order of reaction with respect to hydrogen product, from −1.7 for Co/Ce(80/20) to −1.4 for 0.5%Ba–CoCe(80/20) (Fig. 9C). These results suggest that the ammonia decomposition reaction on CoCe catalysts is limited by competitive adsorption of H_2 on the active sites and/or the re-hydrogenation of the NH_x intermediates.[51,52] According to our kinetic analysis, addition of Ba alleviates this limitation to a certain degree, most likely by decreasing the H_2 affinity of cobalt[53–55] as well as by the increase in the basic properties of the catalyst surface, weakening the H_2 adsorption and limiting the H_2 poisoning.[46,56,57] The XPS measurements confirmed that no electronic effect induced by the addition of Ba is expected, since there was no change in the Co binding energy in the sample

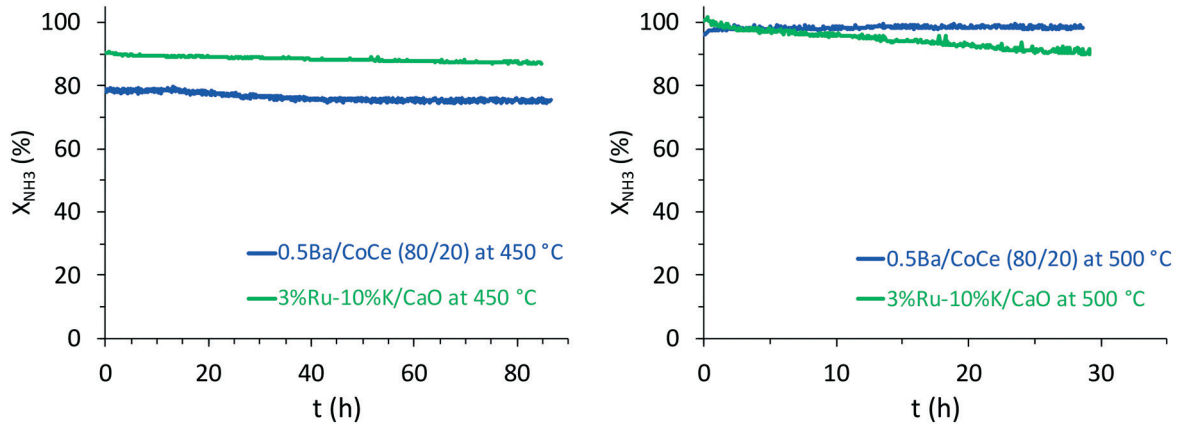

Fig. 8 Time dependence of the catalytic activity of 0.5%Ba–CoCe(80/20) and Ru-based catalyst for stability testing. Reaction conditions: T = 450–500 °C; P = 1 atm; NH_3 flow rate 30 Nml min^{-1}; W_{cat} = 200 mg; WHSV = 9000 mL g^{-1} h^{-1}.

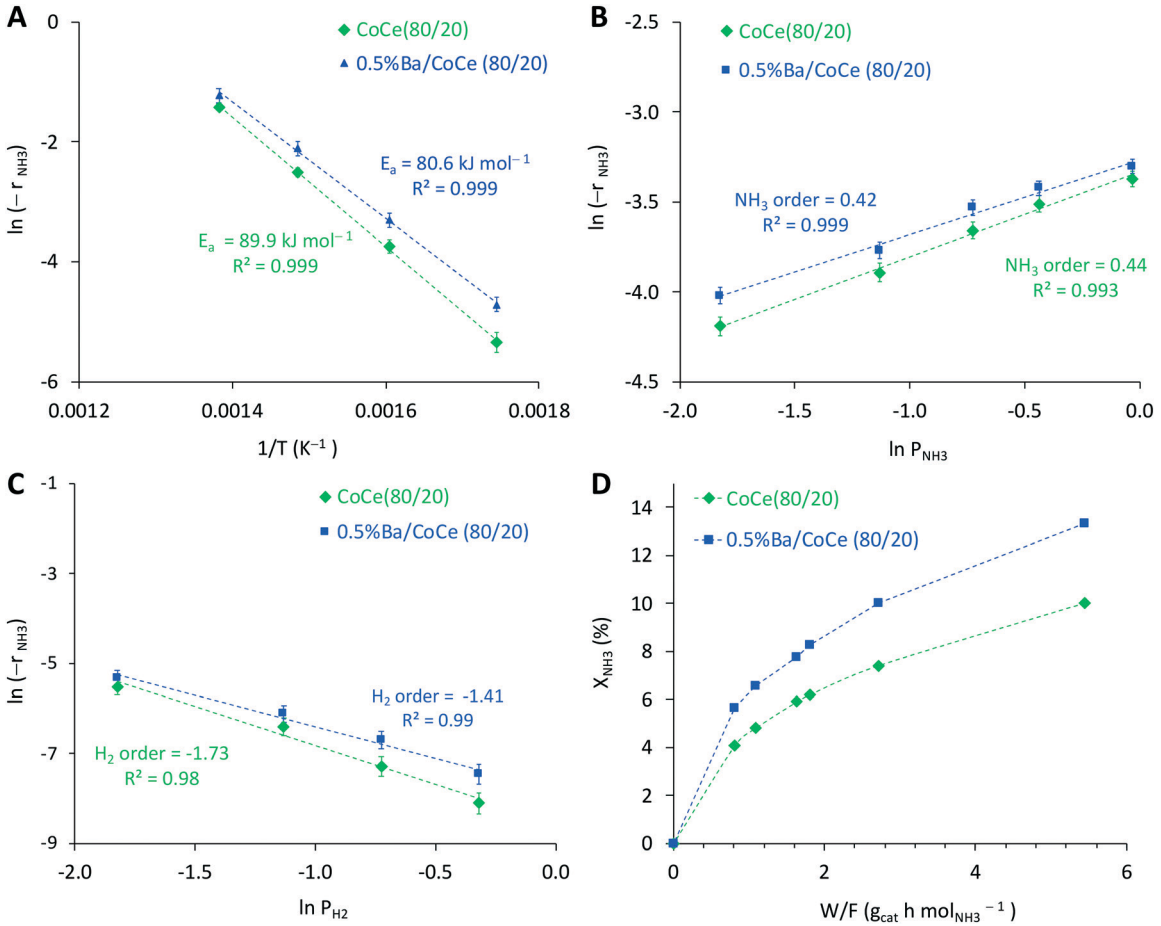

Fig. 9 Kinetic parameters of the 0.5%Ba–Co/Ce(80/20) and Co/Ce(80/20) catalysts. (A) Arrhenius plots in the temperature range 250–400 °C at atmospheric pressure. Dependence of NH_3 decomposition rate on the partial pressures of NH_3 (B) and H_2 (C); conversion *vs.* contact time (D) at 350 °C and P_{atm}. Reaction rate ($-r_{NH_3}$) in mol g^{-1} h^{-1}.

with Ba. However, the presence of the partially reduced Ce, together with the presence of the extremely small Ce clusters, could modify the electron density of the Co species, at least locally. It has been previously reported that partially reduced lanthanide oxides (CeO_2 or La_2O_3) donate electrons to Ru or Co species.[40,58,59] This effect would change the interaction with the reaction intermediates and might be responsible for the lower hydrogen inhibition found for the CoCe catalysts promoted with Ba.

Conclusions

Barium-promoted cobalt–cerium catalysts prepared by coprecipitation are very efficient and stable at decomposing ammonia. When promoted with Ba, the sample with the optimal Co/Ce molar ratio, 0.5 wt% Ba–CoCe(80/20), shows a comparable catalytic performance to that of Ru-based benchmark catalysts at temperatures as low as 450 °C. The stability of the catalyst under the reaction conditions demonstrates a great application potential for the production of CO_x-free hydrogen.

Extensive characterization and in-depth kinetic analyses revealed the crucial role of Ce as a structural promoter, improving Co dispersion and preventing aggregation and sintering even under reaction conditions. Furthermore, addition of Ba decreases the H_2 affinity of the Co active phase, lowering the activation energy of the reaction and alleviating the negative effect of slow hydrogen desorption from the active sites. Overall, coprecipitation is shown to result in unique catalytic architectures with enhanced catalytic performance. This approach may open the door to the synthesis of superior (and cheaper) catalysts based on more abundant transition metals such as Fe or Ni.[60,61]

Conflicts of interest

There are no conflicts to declare.

Acknowledgements

The authors gratefully acknowledge the financial support provided by Saudi Aramco and the resources and facilities

provided by the King Abdullah University of Science and Technology.

References

1 A. Klerke, C. H. Christensen, J. K. Nørskov and T. Vegge, Ammonia for hydrogen storage: challenges and opportunities, *J. Mater. Chem.*, 2008, **18**(20), 2304–2310.
2 F. Schüth, R. Palkovits, R. Schlögl and D. S. Su, Ammonia as a possible element in an energy infrastructure: catalysts for ammonia decomposition, *Energy Environ. Sci.*, 2012, **5**(4), 6278–6289.
3 S. F. Yin, B. Q. Xu, X. P. Zhou and C. T. Au, A mini-review on ammonia decomposition catalysts for on-site generation of hydrogen for fuel cell applications, *Appl. Catal., A*, 2004, **277**(1), 1–9.
4 C. H. Christensen, T. Johannessen, R. Z. Sørensen and J. K. Nørskov, Towards an ammonia-mediated hydrogen economy?, *Catal. Today*, 2006, **111**(1), 140–144.
5 T. E. Bell and L. Torrente-Murciano, H2 Production via Ammonia Decomposition Using Non-Noble Metal Catalysts: A Review, *Top. Catal.*, 2016, **59**(15), 1438–1457.
6 X. Duan, X. Zhou and D. Chen, Structural manipulation of the catalysts for ammonia decomposition, in *Catalysis: Volume 25*, The Royal Society of Chemistry, 2013, vol. 25, pp. 118–140.
7 E. García-Bordejé, S. Armenise and L. Roldán, Toward Practical Application Of H2 Generation From Ammonia Decomposition Guided by Rational Catalyst Design, *Catal. Rev.: Sci. Eng.*, 2014, **56**(2), 220–237.
8 S. Mukherjee, S. V. Devaguptapu, A. Sviripa, C. R. F. Lund and G. Wu, Low-temperature ammonia decomposition catalysts for hydrogen generation, *Appl. Catal., B*, 2018, **226**, 162–181.
9 G. Thomas and G. Parks, *Potential Roles of Ammonia in a Hydrogen Economy. Annual DOE hydrogen program merit review*, U.S. Department of Energy, 2006.
10 A. Boisen, S. Dahl, J. K. Nørskov and C. H. Christensen, Why the optimal ammonia synthesis catalyst is not the optimal ammonia decomposition catalyst, *J. Catal.*, 2005, **230**(2), 309–312.
11 C. J. H. Jacobsen, S. Dahl, B. S. Clausen, S. Bahn, A. Logadottir and J. K. Nørskov, Catalyst Design by Interpolation in the Periodic Table: Bimetallic Ammonia Synthesis Catalysts, *J. Am. Chem. Soc.*, 2001, **123**(34), 8404–8405.
12 Y.-Q. Gu, Z. Jin, H. Zhang, R.-J. Xu, M.-J. Zheng, Y.-M. Guo, Q.-S. Song and C.-J. Jia, Transition metal nanoparticles dispersed in an alumina matrix as active and stable catalysts for COx-free hydrogen production from ammonia, *J. Mater. Chem. A*, 2015, **3**(33), 17172–17180.
13 Z. Lendzion-Bielun, U. Narkiewicz and W. Arabczyk, Cobalt-based Catalysts for Ammonia Decomposition, *Materials*, 2013, **6**(6), 2400–2409.
14 S. Podila, Y. A. Alhamed, A. A. AlZahrani and L. A. Petrov, Hydrogen production by ammonia decomposition using Co catalyst supported on Mg mixed oxide systems, *Int. J. Hydrogen Energy*, 2015, **40**(45), 15411–15422.
15 S. Podila, H. Driss, S. F. Zaman, Y. A. Alhamed, A. A. AlZahrani, M. A. Daous and L. A. Petrov, Hydrogen generation by ammonia decomposition using Co/MgO–La2O3 catalyst: Influence of support calcination atmosphere, *J. Mol. Catal. A: Chem.*, 2016, **414**, 130–139.
16 D. Varisli and N. G. Kaykac, COx free hydrogen production over cobalt incorporated silicate structured mesoporous catalysts, *Appl. Catal., B*, 2012, **127**, 389–398.
17 D. Varisli and N. G. Kaykac, Hydrogen from ammonia over cobalt incorporated silicate structured catalysts prepared using different cobalt salts, *Int. J. Hydrogen Energy*, 2016, **41**(14), 5955–5968.
18 L. H. Yao, Y. X. Li, J. Zhao, W. J. Ji and C. T. Au, Core–shell structured nanoparticles(M@SiO2, Al2O3, MgO; M=Fe, Co, Ni, Ru) and their application in COx-free H2 production via NH3 decomposition, *Catal. Today*, 2010, **158**(3), 401–408.
19 Ł. Czekajło and Z. Lendzion-Bieluń, Effect of preparation conditions and promoters on the structure and activity of the ammonia decomposition reaction catalyst based on nanocrystalline cobalt, *Chem. Eng. J.*, 2016, **289**, 254–260.
20 H. A. Lara-García, J. A. Mendoza-Nieto, H. Pfeiffer and L. Torrente-Murciano, COx-free hydrogen production from ammonia on novel cobalt catalysts supported on 1D titanate nanotubes, *Int. J. Hydrogen Energy*, 2019, **44**(57), 30062–30074.
21 A. Srifa, K. Okura, T. Okanishi, H. Muroyama, T. Matsui and K. Eguchi, Hydrogen production by ammonia decomposition over Cs-modified Co3Mo3N catalysts, *Appl. Catal., B*, 2017, **218**, 1–8.
22 L. Li, R. Jiang, W. Chu, H. Cang, H. Chen and J. Yan, Cobalt nanoparticles embedded in a porous carbon matrix as an efficient catalyst for ammonia decomposition, *Catal. Sci. Technol.*, 2017, **7**(6), 1363–1371.
23 L. Li, L. Sun, H. Cang, W. Chu, J. Shao and J. Yan, Silica-assisted mesoporous Co@Carbon nanoplates derived from ZIF-67 crystals and their enhanced catalytic activity, *J. Solid State Chem.*, 2018, **267**, 134–139.
24 H. Zhang, Y. A. Alhamed, W. Chu, Z. Ye, A. AlZahrani and L. Petrov, Controlling Co-support interaction in Co/MWCNTs catalysts and catalytic performance for hydrogen production via NH3 decomposition, *Appl. Catal., A*, 2013, **464–465**, 156–164.
25 J. Zhang, M. Comotti, F. Schüth, R. Schlögl and D. S. Su, Commercial Fe- or Co-containing carbon nanotubes as catalysts for NH3 decomposition, *Chem. Commun.*, 2007(19), 1916–1918.
26 R. Can Seyfeli and D. Varisli, Ammonia decomposition reaction to produce COx-free hydrogen using carbon supported cobalt catalysts in microwave heated reactor system, *Int. J. Hydrogen Energy*, 2020, 34867–34878.
27 L. Torrente-Murciano, A. K. Hill and T. E. Bell, Ammonia decomposition over cobalt/carbon catalysts—Effect of carbon support and electron donating promoter on activity, *Catal. Today*, 2017, **286**, 131–140.

28 S. Sayas, N. Morlanés, S. P. Katikaneni, A. Harale, B. Solami and J. Gascon, High pressure ammonia decomposition on Ru–K/CaO catalysts, *Catal. Sci. Technol.*, 2020, **10**(15), 5027–5035.

29 X. Ju, L. Liu, P. Yu, J. Guo, X. Zhang, T. He, G. Wu and P. Chen, Mesoporous Ru/MgO prepared by a deposition-precipitation method as highly active catalyst for producing COx-free hydrogen from ammonia decomposition, *Appl. Catal., B*, 2017, **211**, 167–175.

30 X. Ju, L. Liu, X. Zhang, J. Feng, T. He, P. Chen and Ru Highly Efficient, MgO Catalyst with Surface-Enriched Basic Sites for Production of Hydrogen from Ammonia Decomposition, *ChemCatChem*, 2019, **11**(16), 4161–4170.

31 A. M. Karim, V. Prasad, G. Mpourmpakis, W. W. Lonergan, A. I. Frenkel, J. G. Chen and D. G. Vlachos, Correlating Particle Size and Shape of Supported Ru/γ-Al2O3 Catalysts with NH3 Decomposition Activity, *J. Am. Chem. Soc.*, 2009, **131**(34), 12230–12239.

32 M. Karolewska, E. Truszkiewicz, B. Mierzwa, L. Kępiński and W. Raróg-Pilecka, Ammonia synthesis over cobalt catalysts doped with cerium and barium. Effect of the ceria loading, *Appl. Catal., A*, 2012, **445–446**, 280–286.

33 A. Tarka, W. Patkowski, M. Zybert, H. Ronduda, P. Wieciński, P. Adamski, A. Sarnecki, D. Moszyński and W. Raróg-Pilecka, Synergistic Interaction of Cerium and Barium-New Insight into the Promotion Effect in Cobalt Systems for Ammonia Synthesis, *Catalysts*, 2020, **10**(6), 658–675.

34 S. S. Y. Lin, D. H. Kim and S. Y. Ha, Metallic phases of cobalt-based catalysts in ethanol steam reforming: The effect of cerium oxide, *Appl. Catal., A*, 2009, **355**(1), 69–77.

35 G. Rambeau, A. Jorti and H. Amariglio, Catalytic activity of a cobalt powder in NH3 synthesis in relation with the allotropic transformation of the metal, *J. Catal.*, 1985, **94**(1), 155–165.

36 B. Lin, Y. Qi, K. Wei and J. Lin, Effect of pretreatment on ceria-supported cobalt catalyst for ammonia synthesis, *RSC Adv.*, 2014, **4**(72), 38093–38102.

37 W. Raróg-Pilecka, M. Karolewska, E. Truszkiewicz, E. Iwanek and B. Mierzwa, Cobalt Catalyst Doped with Cerium and Barium Obtained by Co-Precipitation Method for Ammonia Synthesis Process, *Catal. Lett.*, 2011, **141**(5), 678–684.

38 M. Zybert, A. Tarka, B. Mierzwa, L. Kępiński and W. Raróg-Pilecka, Promotion effect of lanthanum on the Co/La/Ba ammonia synthesis catalysts—the influence of lanthanum content, *Appl. Catal., A*, 2016, **515**, 16–24.

39 A. Parastaev, V. Muravev, E. Huertas Osta, A. J. F. van Hoof, T. F. Kimpel, N. Kosinov and E. J. M. Hensen, Boosting CO2 hydrogenation via size-dependent metal–support interactions in cobalt/ceria-based catalysts, *Nat. Catal.*, 2020, **3**(6), 526–533.

40 B. Lin, Y. Liu, L. Heng, J. Ni, J. Lin and L. Jiang, Effect of ceria morphology on the catalytic activity of Co/CeO2 catalyst for ammonia synthesis, *Catal. Commun.*, 2017, **101**, 15–19.

41 C. Huang, Y. Yu, X. Tang, Z. Liu, J. Zhang, C. Ye, Y. Ye and R. Zhang, Hydrogen generation by ammonia decomposition over Co/CeO2 catalyst: Influence of support morphologies, *Appl. Surf. Sci.*, 2020, **532**, 147335.

42 X. I. Pereira-Hernández, A. DeLaRiva, V. Muravev, D. Kunwar, H. Xiong, B. Sudduth, M. Engelhard, L. Kovarik, E. J. M. Hensen, Y. Wang and A. K. Datye, Tuning Pt-CeO2 interactions by high-temperature vapor-phase synthesis for improved reducibility of lattice oxygen, *Nat. Commun.*, 2019, **10**(1), 1358.

43 M. C. Biesinger, B. P. Payne, A. P. Grosvenor, L. W. M. Lau, A. R. Gerson and R. S. C. Smart, Resolving surface chemical states in XPS analysis of first row transition metals, oxides and hydroxides: Cr, Mn, Fe Co and Ni, *Appl. Surf. Sci.*, 2011, **257**(7), 2717–2730.

44 X.-C. Hu, X.-P. Fu, W.-W. Wang, X. Wang, K. Wu, R. Si, C. Ma, C.-J. Jia and C.-H. Yan, Ceria-supported ruthenium clusters transforming from isolated single atoms for hydrogen production via decomposition of ammonia, *Appl. Catal., B*, 2020, **268**, 118424.

45 R. Kojima and K.-i. Aika, Cobalt molybdenum bimetallic nitride catalysts for ammonia synthesis: Part 1. Preparation and characterization, *Appl. Catal., A*, 2001, **215**(1), 149–160.

46 B. Lin, Y. Liu, L. Heng, J. Ni, J. Lin and L. Jiang, Effect of barium and potassium promoter on Co/CeO2 catalysts in ammonia synthesis, *J. Rare Earths*, 2018, **36**(7), 703–707.

47 S. Hagen, R. Barfod, R. Fehrmann, C. J. H. Jacobsen, H. T. Teunissen, K. Ståhl and I. Chorkendorff, New efficient catalyst for ammonia synthesis: barium-promoted cobalt on carbon, *Chem. Commun.*, 2002, 1206–1207.

48 W. Raróg-Pilecka, A. Jedynak-Koczuk, J. Petryk, E. Miśkiewicz, S. Jodzis, Z. Kaszkur and Z. Kowalczyk, Carbon-supported cobalt–iron catalysts for ammonia synthesis, *Appl. Catal., A*, 2006, **300**(2), 181–185.

49 S. Sartipi, M. Alberts, M. J. Meijerink, T. C. Keller, J. Pérez-Ramírez, J. Gascon and F. Kapteijn, Towards Liquid Fuels from Biosyngas: Effect of Zeolite Structure in Hierarchical-Zeolite-Supported Cobalt Catalysts, *ChemSusChem*, 2013, **6**(9), 1646–1650.

50 A. Tarka, M. Zybert, Z. Kindler, J. Szmurło, B. Mierzwa and W. Raróg-Pilecka, Effect of precipitating agent on the properties of cobalt catalysts promoted with cerium and barium for NH3 synthesis obtained by Co-precipitation, *Appl. Catal., A*, 2017, **532**, 19–25.

51 S. Armenise, E. García-Bordejé, J. L. Valverde, E. Romeo and A. Monzón, A Langmuir–Hinshelwood approach to the kinetic modelling of catalytic ammonia decomposition in an integral reactor, *Phys. Chem. Chem. Phys.*, 2013, **15**(29), 12104–12117.

52 G. Djéga-Mariadassou, C.-H. Shin and G. Bugli, Tamaru's model for ammonia decomposition over titanium oxynitride, *J. Mol. Catal. A: Chem.*, 1999, **141**(1), 263–267.

53 C. G. Visconti, M. Martinelli, L. Falbo, A. Infantes-Molina, L. Lietti, P. Forzatti, G. Iaquaniello, E. Palo, B. Picutti and F. Brignoli, CO2 hydrogenation to lower olefins on a high surface area K-promoted bulk Fe-catalyst, *Appl. Catal., B*, 2017, **200**, 530–542.

54 J. Xie, P. P. Paalanen, T. W. van Deelen, B. M. Weckhuysen, M. J. Louwerse and K. P. de Jong, Promoted cobalt metal catalysts suitable for the production of lower olefins from natural gas, *Nat. Commun.*, 2019, **10**(1), 167.

55 R.-P. Ye, J. Ding, W. Gong, M. D. Argyle, Q. Zhong, Y. Wang, C. K. Russell, Z. Xu, A. G. Russell, Q. Li, M. Fan and Y.-G. Yao, CO2 hydrogenation to high-value products via heterogeneous catalysis, *Nat. Commun.*, 2019, **10**(1), 5698.

56 Y. Im, H. Muroyama, T. Matsui and K. Eguchi, Ammonia decomposition over nickel catalysts supported on alkaline earth metal aluminate for H2 production, *Int. J. Hydrogen Energy*, 2020, **45**(51), 26979–26988.

57 R. Kojima and K.-I. Aika, Cobalt molybdenum bimetallic nitride catalysts for ammonia synthesis: Part 2 Kinetic study, *Appl. Catal., A*, 2001, **218**(1), 121–128.

58 Y. Izumi, Y. Iwata and K.-I. Aika, Catalysis on Ruthenium Clusters Supported on CeO2 or Ni-Doped CeO2: Adsorption Behavior of H2 and Ammonia Synthesis, *J. Phys. Chem.*, 1996, **100**(22), 9421–9428.

59 Y. Niwa and K.-I. Aika, The Effect of Lanthanide Oxides as a Support for Ruthenium Catalysts in Ammonia Synthesis, *J. Catal.*, 1996, **162**(1), 138–142.

60 P. Xie, Y. Yao, Z. Huang, Z. Liu, J. Zhang, T. Li, G. Wang, R. Shahbazian-Yassar, L. Hu and C. Wang, Highly efficient decomposition of ammonia using high-entropy alloy catalysts, *Nat. Commun.*, 2019, **10**(1), 4011.

61 L. Huo, B. Liu, H. Li, B. Cao, X.-C. Hu, X.-P. Fu, C. Jia and J. Zhang, Component synergy and armor protection induced superior catalytic activity and stability of ultrathin Co-Fe spinel nanosheets confined in mesoporous silica shells for ammonia decomposition reaction, *Appl. Catal., B*, 2019, **253**, 121–130.